

COMPUTATIONAL STUDY OF SUPERSONIC FLOW OVER A FLAT PLATE WITH PROTRUSION

Vikram Deshpande
Research Scholar
Department of Applied Mechanics
Indian Institute of Technology Delhi
Hauz Khas, New Delhi-110 016, India

Sanjeev Sanghi
Professor
Department of Applied Mechanics
Indian Institute of Technology Delhi
Hauz Khas, New Delhi-110 016, India
Email : sanghi@am.iitd.ac.in

Brijesh Eshpuniyani
Assistant Professor
Department of Aerospace Engineering
Indian Institute of Technology Kanpur
Kanpur-208 016, India

Abstract

Motivated by a developmental approach of using micro-actuated surface protrusions to control/maneuver slender bodies in supersonic flight, this paper presents a detailed study of a two dimensional laminar supersonic flow over a flat plate with a surface protrusion. The flow field is computed by solving the Navier-Stokes equations using the finite difference method with the particle velocity upwinding scheme (PVUS) for spatial discretization, and the explicit Mac Cormack scheme for temporal integration. A range of free stream Mach numbers (2.0 - 4.5), Reynolds numbers (1000 - 100000) and protrusion heights (0.866% to 8.66% of the characteristic length) has been considered for a thorough parametric study. The parametric study indicates that the oblique shock structure and strength are influenced by all the variables to varying extents. However, the shock location is substantially altered by the protrusion height, Reynolds number, and protrusion shape, while the influence of Mach number is only marginal. An increase in the protrusion height results in an increased wall pressure as well as increased separation lengths on both sides of the protrusion. In contrast, an increase in Mach number increases the wall pressure, but moves the separation point marginally towards the protrusion. Increase in Reynolds number and protrusion bluntness (triangular \rightarrow trapezoidal \rightarrow rectangular) increases separation lengths on both sides of the protrusion. In addition to taking a close look at the flow physics, particularly in the protrusion vicinity, considerable attention has also been devoted to important design parameters such as wall pressure, skin friction and the overall normal and tangential force coefficients.

Nomenclature

p_{∞}	= Free stream pressure	ρ_{∞}	= Free stream density
T_{∞}	= Free stream temperature	x, y	= Cartesian coordinates
U_{∞}	= Free stream velocity	L	= Characteristic length i.e. distance between leading edge to centre of protrusion
M_{∞}	= Free stream Mach number	γ	= Specific heat ratio
Re_{∞}	= Free stream Reynolds number	C_v	= Specific heat at constant volume
k_{∞}	= Free stream thermal conductivity	p	= Non-dimensional pressure
		T	= Non-dimensional temperature

ρ	= Non-dimensional density
u, v	= Non-dimensional velocity components in x and y direction, respectively
μ	= Non-dimensional viscosity
k	= Non-dimensional thermal conductivity
E	= Non-dimensional total energy
e	= Non-dimensional specific internal energy
C_f	= Skin-friction coefficient
RH	= Relative height of protrusion i.e. ratio of height of protrusion to characteristic length
P_w	= Non-dimensional wall pressure

Introduction

This study is motivated by the long term perspective of using shockwaves to assist or replace conventional control surfaces in maneuvering supersonic vehicles and missiles. One method of creating shockwaves to generate the necessary control forces is via the use of surface protrusions that can emerge into the flow field (possibly using micro-actuation) as and when needed, and withdraw back into the surface at other times to avoid unnecessary drag expenditure. The overall problem of designing suitable control laws based on the fully three dimensional, turbulent dynamics of supersonic flow past moving surface protrusions is an extremely challenging proposition that requires a series of systematic studies. We start by making a set of simplifying assumptions to keep the problem tractable yet relevant, and consider a two-dimensional laminar supersonic flow past a flat plate with surface protrusions of different sizes and shapes. A range of free stream Mach numbers (2.0 - 4.5), Reynolds numbers (1000 - 100000) and protrusion heights (0.866% to 8.66% of the characteristic length) has been considered for a thorough parametric study. The major contributions of the present paper in the direction of motivational objective are: (1) mapping of the overall flow field in terms of the principal features - shock creation, shock intersections, formation of separation bubbles, shock boundary layer interaction, etc., (2) a detailed look at the flow physics, particularly in the protrusion vicinity, and (3) consideration of important design parameters such as wall pressure, skin friction and the overall normal and tangential force coefficients.

Research on utilization of micro actuator arrays for flow control has received considerable attention in the recent past [1-3]. Anderson et al. [1] focused on the design and development of high pay-off advanced technology approaches for mixed compression inlets operating in the two to four Mach number regime. The study was aimed at

establishing the ability of micro array flow control to manage shock wave turbulent boundary layer interaction in supersonic inlets, as well as evaluating the effectiveness of this strategy in comparison to conventional boundary layer bleed systems. Three different micro devices were considered: standard micro vanes, tapered micro vanes and standard micro ramp arrays. The effects of all three types of micro array devices were examined using a shock pressure rise induced by a 10 degree shock generator at a free stream Mach number of two. All devices showed that the boundary layer displacement thickness downstream of the shock wave boundary layer interaction was substantially larger with micro actuator flow control than with conventional boundary layer bleed control.

In contrast, in the subsonic regime, Huang et al. [2] investigated the application of micro actuator arrays for macro fluidic control using a delta wing model in a wind tunnel. In general, delta wing leading edges create symmetric pairs of primary and secondary vortices. Controlling the separation of the boundary layer using micro actuators at the leading edge can allow us to control the location of the vortex pairs, which in turn can allow us to manipulate the pressure field around the wing/aircraft. It was hypothesized in the study that the vortex shifting mechanisms with micro actuators can be used to replace or supplement conventional control surfaces at high angle of attack, where these become ineffective due to trailing edge separation of the flow. For example, it was experimentally shown that although conventional ailerons have a chord of about 19.4% of the mean aerodynamic chord, a micro actuator of only 0.8% of the mean aerodynamic chord could generate rolling moment coefficients of about 50% of that generated by conventional ailerons.

Further, an experimental investigation on active flow control concept utilizing miniature deployable structures for advanced weapons control was carried out by Patel et al. [3]. The study aimed at providing pitch and yaw control to weapons (slender bodies) that operate at low angles of attack, where the baseline control is primarily provided by tail-fins. The miniature-spoilers, integrated on the weapon boat-tail and fins were made to act as flow control devices to provide aerodynamic control. The results of the study indicated that this technology offers an active, compact, light-weight, flight control system for aerodynamic maneuvering, and is applicable to all types of slender-bodied weapons including missiles, projectiles, and munitions.

Flow over a flat plate with a ramp/wedge/hump has been studied theoretically, experimentally and numeri-

cally by various researchers with an intention of understanding the different aspects of flow separation, shock boundary layer interactions, avoidance or delay in flow separation, etc. Smith [4] considered limiting cases of very small to very large humps, and the solution was arrived at mathematically using a Triple Deck theory. The flow was found to be qualitatively similar for all hump sizes in the subsonic as well as the supersonic speed regimes. The distribution of pressure gradient and the skin friction were found to be to first order of height of protrusion for both subsonic and supersonic flows. Similarly were the wake solutions in subsonic regime. Dolling and Murphy [5] experimentally studied supersonic flow past a compression ramp to investigate shockwave turbulent boundary layer interaction. They observed that the flow separated upstream of the ramp and reattached down stream of the corner, forming a separation bubble at the corner of the ramp. Large amplitude pressure fluctuations were seen near separation and reattachment points. The separation shock wave structure was found to be highly unsteady generating an intermittent wall pressure signal in this vicinity. Chapman et al. [6] carried out an extensive experimental investigation of supersonic flow over a flat plate with obstructions like forward and backward facing steps, compression ramps and curved surfaces with and without a turbulent trip. The main aim of their investigation was to study the phenomena of flow separation and transition from laminar to turbulence. The scope of measurement encompassed Mach numbers between 0.4 and 3.6, and Reynolds numbers, based on length in front of the obstruction, between 4×10^3 to 5×10^6 . For a given model shape, the location of transition relative to the reattachment and separation positions is dominant in controlling the characteristic features of pressure distribution irrespective of Mach number and Reynolds number. This dominance leads to classification of each separated flow into one of three types i.e. pure laminar, transition and turbulent. The pure laminar separations (transition downstream of reattachment zone) and turbulent separations (transition upstream of separation) were relatively steady and depended only to a small extent on Reynolds number. However, transitional separations (transition between separation and reattachment) generally were unsteady and often depended markedly on Reynolds number. In transitional separations an abrupt pressure rise often occurs at the location of transition, especially when transition is only a short distance upstream of reattachment. Efimtsov et al. [7] carried out a series of experimental investigations on the TU-144LL Flying Laboratory and obtained flight-test data of the pressure fluctuation field in front of a forward-facing step and behind a backward-facing step.

The flight test covered a Mach number range of 0.57 - 1.97, step heights of 4 mm and 7 mm. The spectral analysis of pressure fluctuations was dependant on mach number. However the effect of Reynolds number on the pressure fluctuation was insignificant.

Carter [8] obtained a numerical solution of the Navier-Stokes equations for laminar supersonic flow past compression corners of 5, 7.5 and 10 deg at Mach 3.0. The solid wall temperature was fixed at free stream stagnation temperature. The flow separation and reattachment was noticed only in case of flow 10 deg compression corner. The flow also exhibited an increase in the displacement thickness near the corner. Degani et al. [9] carried out comparison between thin layer and Navier-Stoke Equations for supersonic flow past a compression corner. The study was carried out at Re of 63×10^6 and a free stream mach number of 2.85 for ramp angles of 20° and 24° . The results of the study confirmed the validity of thin layer model for such a class of problems. The discrepancies in the results of thin layer and N-S simulations were minor and confined only to the separation bubble region. Examination of time development of this region showed that a truly steady solution is not only difficult to achieve, but is obtained only after a large number of time steps and by use of sufficiently high values of smoothing coefficients. Hung and Mac Cormack [10] developed an efficient time-splitting, second-order accurate, numerical scheme that was used to solve the complete N-S equation for supersonic and hypersonic laminar flow over a two-dimensional compression corner. Their results indicated that the pressure profile is neither constant across the boundary layer nor constant along simple straight characteristic lines, as had been assumed in some previous analyses. Qamar et al. [11] developed an innovative, low cost and efficient upwind scheme which was based on the single parameter i.e. Particle Velocity. The scheme is named as Particle Velocity Upwinding (PVU) scheme. After testing the scheme for different test cases, the authors have carried out a detailed numerical investigation of the forward-facing step for step heights of 10% and 20% of the characteristic length, stream Mach numbers from 1.5 to 3.5 with Reynolds number fixed at $Re=1 \times 10^4$. The study showed that the strength and the location of the oblique shock are affected by two parameters: (1) the free stream Mach number, and (2) the step height H . It is also shown that the shock strength is significantly affected by the step height, as well as the free stream Mach number. However, the shock location is altered significantly only by the step height.

The present work considers a model problem of supersonic flow over a flat plate with different shaped protrusions. This allows us to consider situations that involve a compression of the oncoming supersonic flow, thus introducing shock wave boundary layer interaction, as well as its subsequent expansion and separation as the flow traverses over the protrusion. The flow field is computed by solving the Navier-Stokes equations using the finite difference method with the particle velocity upwinding scheme (PVUS) for spatial discretization, and the explicit Mac Cormack scheme for temporal integration. The governing equations with the numerical scheme and computational domain/setup employed for the simulations are described in Section II. Section III presents a detailed discussion and analysis of results obtained for a triangular protrusion for a wide range of parameters. Section IV compares the flow features and force coefficients observed for a triangular protrusion with trapezoidal and rectangular protrusions. Finally, the conclusions drawn from the study are presented in Section V.

Numerical Procedure and Computational Setup

Governing Equations

The two-dimensional Navier-Stokes equations transformed into a generalized coordinate system, neglecting body forces and volumetric heating, in their strong conservative form are discretised using a finite difference methodology on a structured grid as described in [9]. The non dimensional form of the governing equations expressed in vector notation is:

$$\frac{\partial U}{\partial t} + \frac{\partial (F^C + F^D)}{\partial \xi} + \frac{\partial (G^C + G^D)}{\partial \eta} = 0 \quad (1)$$

Here, the flux vectors F and G are split into two parts, the convective part (F^C and G^C) and the diffusive part (F^D and G^D). The convective part consists of the convective flux in each equation, whereas all other parts of F and G vectors (pressure and viscous terms) are included in the diffusive part. Thus, in terms of vector notation,

$$U = \begin{Bmatrix} \rho \\ \rho u \\ \rho v \\ \rho E \end{Bmatrix}; F^C = \begin{Bmatrix} v^\xi \rho \\ v^\xi \rho u \\ v^\xi \rho v \\ v^\xi \rho E \end{Bmatrix}; G^C = \begin{Bmatrix} v^\eta \rho \\ v^\eta \rho u \\ v^\eta \rho v \\ v^\eta \rho E \end{Bmatrix}$$

$$F^D = \begin{Bmatrix} 0 \\ H_1 \xi_x + Q_1 \xi_y \\ H_2 \xi_x + Q_2 \xi_y \\ H_3 \xi_x + Q_3 \xi_y \end{Bmatrix}; G^D = \begin{Bmatrix} 0 \\ H_1 \eta_x + Q_1 \eta_y \\ H_2 \eta_x + Q_2 \eta_y \\ H_3 \eta_x + Q_3 \eta_y \end{Bmatrix} \quad (2)$$

E is the non dimensional total energy which combines both internal energy and kinetic energy.

$$E = e + \gamma(\gamma - 1) M_\infty^2 (V^2/2) \quad (3)$$

v^ξ and v^η are the contra-variant velocities in the computational domain defined as

$$\begin{aligned} v^\xi &= u \xi_x + v \xi_y \\ v^\eta &= u \eta_x + v \eta_y \end{aligned} \quad (4)$$

The others symbols are defined as follows:

$$H_1 = \frac{p}{\gamma M_\infty^2} - \frac{2}{3} \frac{\mu}{Re_\infty} (2\delta_x(u) - \delta_y(v))$$

$$H_2 = -\frac{\mu}{Re_\infty} (\delta_x(v) + \delta_y(u))$$

$$H_3 = -\frac{\gamma k}{Pr_\infty Re_\infty} (\delta_x(T)) + (\gamma - 1) \rho u$$

$$-\frac{2}{3} \frac{\gamma(\gamma - 1) u \mu M_\infty^2}{Re_\infty} (2\delta_x(u) - \delta_y(v))$$

$$-\frac{\gamma(\gamma - 1) v \mu M_\infty^2}{Re_\infty} (\delta_y(u) + \delta_x(v))$$

$$Q_1 = -\frac{\mu}{Re_\infty} (\delta_x(v) + \delta_y(u))$$

$$Q_2 = \frac{p}{\gamma M_\infty^2} - \frac{2}{3} \frac{\mu}{Re_\infty} (2\delta_y(v) - \delta_x(u))$$

$$Q_3 = -\frac{\gamma k}{Pr_\infty Re_\infty} (\delta_y(T)) + (\gamma - 1) \rho v$$

$$-\frac{2}{3} \frac{\gamma(\gamma-1) \nu \mu M_\infty^2}{Re_\infty} (2\delta_y(v) - \delta_x(u)) - \frac{\gamma(\gamma-1) u \mu M_\infty^2}{Re_\infty} (\delta_y(u) + \delta_x(v)) \quad (5)$$

where,

$$\delta_x(\cdot) = \frac{\partial}{\partial \xi} \xi_x + \frac{\partial}{\partial \eta} \eta_x :$$

$$\delta_y(\cdot) = \frac{\partial}{\partial \xi} \xi_y + \frac{\partial}{\partial \eta} \eta_y$$

The viscosity of the fluid changes with temperature. Assuming a calorifically perfect gas, Sutherland law is typically used to calculate the local viscosity. μ_o and T_o are reference values at standard sea level conditions. Sutherland Law of dynamic viscosity is given by:

$$\mu(T) = T^{3/2} \left(\frac{T_\infty + S^*}{T T_\infty + S^*} \right) \quad (6)$$

where, $S^* = 123.6$ K, Sutherland constant.

Various flow field variables are non-dimensionalised with respect to the following scales and then transformed into generalized coordinate system.

$$e = \frac{\bar{e}}{C_v T_\infty}, \quad t = \frac{\bar{t} U_\infty}{L}, \quad x = \frac{\bar{x}}{L}, \quad y = \frac{\bar{y}}{L},$$

$$u = \frac{\bar{u}}{U_\infty}, \quad v = \frac{\bar{v}}{U_\infty}, \quad p = \frac{\bar{p}}{P_\infty}, \quad T = \frac{\bar{T}}{T_\infty},$$

$$\mu = \frac{\bar{\mu}}{\mu_\infty}, \quad k = \frac{\bar{k}}{k_\infty}, \quad E = \frac{\bar{E}}{C_v T_\infty} \quad (7)$$

The subscript ∞ represents the incoming free stream conditions and the over bar values represent the corresponding dimensional values. L is some appropriate reference length, i.e. distance between leading edge and the centre of the protrusion.

Equation (1) is marched in time by a predictor and corrector method. After a series of simulations with progressively smaller time steps to ensure convergence and

repeatability, a considerably small time step of 5×10^{-5} has been used. However for simulations of Reynolds number equal to 1×10^5 , the initial time steps were as small as 8×10^{-6} . Subsequently, the same was gradually increased to 5×10^{-5} . The solution vector at any point (i, j) of the grid at the new time level $(n+1)$ is obtained explicitly through the following predictor and corrector steps:

Predictor step:

$$U^* = U^n - \Delta t \left\{ (\delta_\eta^- F^c)^n + (\delta_\eta^+ F^d)^n + \left\{ (\delta_\xi^- G^c)^n + (\delta_\xi^+ G^d)^n \right\} \right\} \quad (8)$$

Corrector step:

$$U^{n+1} = \frac{U^* + U^n}{2} - \frac{1}{2} \Delta t \left\{ (\delta_\eta^- F^c)^* + (\delta_\eta^+ F^d)^* + \left\{ (\delta_\xi^- G^c)^* + (\delta_\xi^+ G^d)^* \right\} \right\} \quad (9)$$

where δ_0^+ , δ_0^- , and δ_0 are the forward, backward and central differencing operators, respectively, with the central differencing operator calculating the difference on the cell faces i.e. between $i+1/2$ and $i-1/2$ values. The schematic diagram of a computational molecule is shown in Fig.1.

Upwind Scheme

A Particle Upwinding Scheme developed by Qamar et al. [11] and Qamar [12] is used for computations. The scheme is second order accurate at all locations except in regions of discontinuities. The discontinuities or regions of steep gradients are detected by employing a smoothness indicator function as employed in WENO schemes. The brief description of the upwind scheme is given by:

First Order Scheme

$$F_{i-\frac{1}{2},j}^C = \begin{cases} u_{i-\frac{1}{2},j} \phi_{i-\frac{1}{2},j}^C & \text{if } u_{i-\frac{1}{2},j} \geq 0 \\ u_{i-\frac{1}{2},j} \phi_{ij}^C & \text{if } u_{i-\frac{1}{2},j} < 0 \end{cases}$$

Where,

$$\phi^F = \begin{Bmatrix} \rho \\ \rho u \\ \rho v \\ \rho E \end{Bmatrix}, \quad (10a)$$

Second Order Scheme

$$(F_c)_{i+1/2,j} = \begin{cases} u_{i+1/2,j} (\alpha_1 \phi_{i+1} + \alpha_2 \phi_i - \alpha_3 \phi_{i-1}) & \text{if } u_{i+1/2,j} \geq 0 \\ u_{i+1/2,j} (\alpha_4 \phi_{i+1} + \alpha_5 \phi_i - \alpha_6 \phi_{i+2}) & \text{if } u_{i+1/2,j} < 0 \end{cases} \quad (10b)$$

$$\alpha_1 = \frac{(\Delta x_{i+1}) (\Delta x_{i+1} + 2\Delta x_{i-1})}{4 (\Delta x_{i+1}) (\Delta x_{i+1} + \Delta x_{i-1})}$$

$$\alpha_2 = \frac{(\Delta x_{i+1}) (\Delta x_{i+1} + 2\Delta x_{i-1})}{4 (\Delta x_{i+1}) (\Delta x_{i-1})}$$

$$\alpha_3 = \frac{(\Delta x_{i+1}) (\Delta x_{i+1})}{4 (\Delta x_{i-1}) (\Delta x_{i+1} + \Delta x_{i-1})}$$

$$\alpha_4 = \frac{(\Delta x_{i+1}) (\Delta x_{i+1} + 2\Delta x_{i+2})}{4 (\Delta x_{i+2}) (\Delta x_{i+1})}$$

$$\alpha_5 = \frac{(\Delta x_{i+1}) (\Delta x_{i+1} + 2\Delta x_{i+2})}{4 (\Delta x_{i+1}) (\Delta x_{i+1} + \Delta x_{i+2})}$$

$$\alpha_6 = \frac{(\Delta x_{i+1}) (\Delta x_{i+1})}{4 (\Delta x_{i+2}) (\Delta x_{i+1} + \Delta x_{i+2})}$$

Where,

$$u_{i+1/2,j} = \frac{(\Delta x_{i+1}) (\Delta x_{i+1} + 2\Delta x_{i-1})}{4 (\Delta x_{i+1}) (\Delta x_{i+1} + \Delta x_{i-1})} u_{i+1}$$

$$+ \frac{(\Delta x_{i+1}) (\Delta x_{i+1} + 2\Delta x_{i-1})}{4 (\Delta x_{i+1}) (\Delta x_{i-1})} u_i$$

$$- \frac{(\Delta x_{i+1}) (\Delta x_{i+1})}{4 (\Delta x_{i-1}) (\Delta x_{i+1} + \Delta x_{i-1})} u_{i-1}$$

$$\Delta x_{i+2} = x_{i+2} - x_{i+1} \quad \Delta x_{i-1} = x_i - x_{i-1} \quad \Delta x_{i+1} = x_{i+1} - x_i$$

In order to detect the discontinuity in the solution domain a smoothness indicator function is utilized given by

$$\varphi(x) = \frac{13}{12} \left\{ \rho_{i-2,j} - 2\rho_{i-1,j} + \rho_{i,j} \right\}^2 + \frac{1}{4} \left\{ \rho_{i-2,j} - 4\rho_{i-1,j} + 3\rho_{i,j} \right\}^2 \quad (11)$$

This is an innovative, low cost and efficient upwind scheme which is based on a single parameter i.e. Particle Velocity. The scheme is second order scheme through out the domain. Although the same is first order at discontinuities, Qamar et al. [11] have proved its efficiency, accuracy and stability in an elaborative manner. The simplicity of this scheme works to our advantage in terms of requirement of lower computational resources without compromising on the accuracy of the results.

Computational Domain

Figure 3 shows the computational domain for the triangular protrusion over a flat plate. The solution domain has been selected in such a fashion so that it includes all of the essential features like shocks, expansion fans, shock/boundary layer interaction and shock-shock interaction that are developed due to the presence of the protrusion. The uniform free stream is aligned with the positive x axis. The solution is obtained in such a way that boundary layer is allowed to develop with time. As a result, the leading-edge boundary-layer shock is generated. The leading edge is placed at $x=0$, and the distance from the leading edge to the vertex of the triangular protrusion $L=1.0$ is used as the characteristic length. At the inflow, pressure, temperature, and Mach number are specified at zero angle of attack. The no-slip condition for velocity is employed at the solid wall, and the wall static temperature is taken to be equal to the free stream air static temperature. The pressure at the solid wall is computed by using the normal momentum equation. At the outflow boundary, the second derivative of pressure, the first derivatives of temperature and velocity are set to zero normal to the boundary. At the top boundary, the first derivatives of all of the flow field variables, u , v , P and T , in the y direction are assumed to be vanishing. The PVU scheme developed by Qamar et al. [11] is applied to the triangular obstruction problem which was proved to be an efficient scheme requiring least computational efforts. A Newtonian fluid (air) with a calorically perfect gas assumption is used for the solution of the full conservative form of the

NavierStokes equation. This problem comprises many parameters that can be varied.

The important parameters that affect the flow are (a) M_∞ , the free stream Mach number (b) Re_∞ , the Reynolds number based on the characteristic length L (c) RH, the ratio of protrusion height and characteristic length Thus, the numerical study involves the variation of Mach number M_∞ in supersonic ranges from 2.0 to 4.5 in steps of 0.5 Mach for five protrusion heights $RH = 0.866\%$, 2.598% , 4.33% , 6.06% and 8.66% , respectively. The simulation was done for three Reynolds numbers Re_∞ equal to 10^3 , 10^4 and 10^5 . The numerical values of other parameters are as follows: $P_\infty = 101,325 \text{ N/m}^2$, $T_\infty = 288 \text{ K}$, $\gamma = 1.4$, $R = 287 \text{ J/(kg K)}$, and $Pr_\infty = 0.716$.

Validation of Code

The code and the scheme is validated for a mile stone test case of Carter [8] i.e. a supersonic two-dimensional viscous flow past the 10-deg compression corner for $Re_\infty = 1.68 \times 10^4$ and $M_\infty = 3.0$. The separation point of the flow for the present computation is at $x = 0.88$, which closely matches with that predicted by Hung and Mac Cormack [10]. Fig.2 show the variation of wall pressure on the wall. The results compare quite well with Carter [8]. This test problem proves the ability of the code and scheme for the computation of flows that involve shock-wave/boundary-layer interaction, which is an important feature of compressible viscous flows.

Grid and Time Independency Study

The computational domain spanned up to 1.75 times the characteristic length horizontally with protrusion vertex at $X=1.0$. The height of the domain was kept at 1.2 times the characteristic length. The grid independence check was carried out for three different grid sizes i.e. 175×121 , 351×201 and 701×251 . The average tangential force obtained was compared with each other. The result yielded by grid 351×201 is found to vary about 6.5% and

2.3% with grid sizes 175×121 and 701×251 respectively. Hence grid size 351×201 used to for entire computations. Table of results is as shown in Table-1.

The non-uniform grid points were distributed in y direction (exponentially varying from 2.65×10^{-3} to 8.632×10^{-3}) to capture the high velocity gradients in the viscous layer near solid wall. However, grid points were spaced uniformly in X direction at spacing of 5.0×10^{-3} . The initial grid generated through algebraic method is rearranged by solving the elliptic Partial Difference Equations as brought out in [13].

Results and Discussions

Spatial Patterns of the Flow Field

Figure 4 is a schematic diagram of the flow features that are developed due to the presence of triangular protrusion. The spatial pattern of the flow field is studied by plotting contours of pressure, temperature, Mach number, and stream trace patterns at $RH = 8.66\%$ and $M_\infty = 3.0$ in Fig.5a to Fig.5d, respectively.

A boundary layer starts developing from the leading edge of the plate, which decelerates the incoming supersonic flow. A weak boundary-layer shock originates from the leading edge of the boundary layer as seen in Fig.5a. Furthermore, all of the compression waves in front of the triangular protrusion merge, leading to a stronger oblique shock well before start of the Protrusion, which can be clearly seen in Fig.5a. An interesting phenomenon can be seen near the vertex of the protrusion i.e. the separation region does not extend till the vertex but ends short of it (this point can be referred as stagnation point where peak pressure on the wall occurs). This leads the flow to negotiate the corner created due to the protrusion and the separated region. Due to such geometry, another oblique shock gets created which is much stronger as compared to previous two shocks. Both the oblique shock-1 and oblique shock-2 interact to form a resultant shock causing the first shock-shock interaction. This resultant oblique

Table-1 : Results of Simulations of Flow Past Triangular Protrusion for Different Grid Sizes

Sl. No.	Grid Size	Tangential Force	Normal Force	% Variation (w.r.t. Grid 'B')	
				Tangential Force	Normal Force
a)	175 x 121	0.779996791	1.29768443	6.5%	1.56%
b)	351 x 201	0.830698848	1.27765918	0.0%	0.0%
c)	701 x 251	0.850084114	1.26734293	2.33%	0.81%

shock merges with the weak leading boundary-layer shock, causing another shock-shock interaction. In both the shock interactions, a single strong shock emerges followed by formation of a weak expansion wave and a slip surface (contact discontinuity).

The oblique shock-1 interacts with the boundary layer in the viscous region near the wall and induces boundary-layer separation. The region between the strong oblique shock and the protrusion is a region of separation, dominated by the presence of a vortex as seen in Fig.5d. A similar flow separation also exists on aft side of the protrusion. However, this flow gets reattached to the flat plate at much shorter distance. At the flow reattachment point on aft side of protrusion, a weak reattachment shock forms. This phenomenon occurs again due to the flow negotiating the corner formed by the separation zone and the flat plate. The temperature contours in Fig.5b indicate the rise in temperature in the vicinity of the shocks. A higher temperature rise is observed at locations where the shocks impinge on the plate. The maximum temperature is observed near the protrusion vertex due to the dissipation of incoming free stream kinetic energy at the reattachment (stagnation) point. The Mach contours in Fig.5c are characterized by a thick band, starting from leading edge to the vertex of the protrusion, and then continuing further till the trailing edge, going around the separated flow regions on both sides of the protrusion. This thick band is the shear layer, which is the region between the outer nearly uniform high-speed flow and the slow-moving recirculating or separated region. This causes a high velocity gradient in the layer, which appears as thick band of concentrated Mach contours.

Effect of Protrusion Height

The effect of protrusion height on the spatial patterns of the flow field is assessed by comparing the spatial patterns for a flat plate (Fig.6a) with those corresponding to relative protrusion heights (*RH*) of 0.866%, 2.598%, 4.33%, 6.06% and 8.66% (Fig.6b-f) of the characteristic length. The free-stream Mach number and Reynolds number are fixed at $M_\infty = 3.0$ and $Re = 10000$ for this set of simulations. Comparing the pressure contour plots, one can conclude that, as the protrusion height increases, the oblique shock-1 moves towards the leading edge. This is also reflected in a plot of wall pressure i.e. $(P_{wall} - P_\infty) / P_\infty$ vs. distance from leading edge (Fig.7). We observe that as the protrusion height increases, not only does the wall pressure increase (due to pressure jump across shock wave), but this increase starts further up-

stream. The sudden wall pressure rise on fore side of the protrusion is an indicator of the location of the stagnation point and oblique shock-2.

Exactly at the vertex of the protrusion, there is an abrupt fall in pressure indicating presence of an expansion region. It is seen from Fig.7a that the wall pressure magnitude behind the protrusion is also altered significantly with increase in protrusion height. In addition, the flow reattaches further downstream for increased protrusion heights as expected. Fig.7b shows the variation of skin friction coefficient for different protrusion heights. The point nearest to the leading edge, where the coefficient of skin friction becomes negative, indicates the beginning of the separation region. Thus, as the protrusion height increases, the separation point shifts toward the leading edge, and, hence, the length of separated region increases with protrusion height.

During each run, the average horizontal and vertical forces on the plate due to pressure and skin friction have been calculated (Fig.8). We observe that the tangential force increases by a factor of 17 to 194 (w.r.t. flat plate values) for relative protrusion heights of 0.866% to 8.66%. Further, the normal force increases up to 11.13% above the flat plate values. With regards to our motivation of investigating the feasibility of using surface protrusions as control mechanisms, the following points get highlighted:

- If such a protrusion is introduced on one side of a flat plate, it results in the generation of asymmetric force which can be effectively utilized for maneuvering of the object moving at supersonic speeds and may replace any conventional control surfaces.
- Similarly, when any control surface of given height exists on the surface then the drag force is continuously being exerted on the body even if there is no requirement of the control force. However, if such a conventional control surface is replaced with the protrusion which can be employed only on need basis, the Drag force will act intermittently resulting in reduced total drag force over complete flight envelope. Lower the total drag force on the body in a given flight envelope, lower will be the propulsive force requirement.

Effect of Free Stream Mach Number

Figures 9a - 9e show the pressure and Mach contours for different Mach numbers at a relative protrusion height

$RH=8.66\%$ and Reynolds number $Re=10000$. An increase in Mach number reduces the inclination of all shocks in the flow fields. It is also observed that increase in Mach number pushes the stronger oblique shock away from the leading edge toward the protrusion. Simultaneously, the reattachment of the flow aft of the protrusion also advances upstream. This results in reduction of the flow separation regions on both sides of the protrusion. Fig.10a to 10b shows the variation of wall pressure and skin friction respectively as a function of distance from leading edge. The movement of the oblique shock and the associated separation point, away from the leading edge, toward the protrusion is clearly seen. The effect of Mach number is more pronounced in the variation of wall pressure as compared to skin friction C_f . The separated zone pressure is significantly increased with increase in free stream Mach number. This is because the strength of the oblique shock increases as the free stream Mach number is increased.

Figures 11a and 11b show the variation of separation lengths (upstream and downstream of protrusion) and peak pressure at the reattachment (stagnation) point on the protrusion with Mach number. The peak pressure on the protrusion increases significantly with an increase in M_∞ (nearly 3.6 times as M_∞ goes from 2.0 to 4.5). In contrast, the separation lengths upstream, downstream, and their sum reduces only by 27%, 49% and 34% respectively. We can thus infer that an increase in Mach number only marginally shifts the shock location.

The average non dimensional tangential and normal forces for various Mach numbers are plotted in Fig.12. We observe that the tangential force increases by a factor of 115 to 351 and the normal force increases from 6.6% to 19.27% (w.r.t. flat plate values) for Mach numbers of 2.0 to 4.5.

Effect of Free Stream Reynolds Number

Figures 13a - 13f show the pressure contours and stream traces at for different Reynolds numbers at a relative protrusion height $RH=8.66\%$ and free stream mach $M_\infty=3.0$. An increase in Reynolds number reduces the inclination of all shocks in the flow fields while moves oblique shock-1 towards leading edge. Similarly, flow reattaches further downstream for increased Reynolds numbers as expected. This results in increase of the flow separation regions on both sides of the protrusion. Fig.14a and 14b shows the variation of wall pressure and skin friction respectively as a function of distance from leading

edge. The movement of the oblique shock and the associated separation point, towards the leading edge and away from protrusion can be seen. The skin friction near the protrusion (i.e. at $x=0.8425$) for $Re_\infty=10^5$ found to change sign from negative to positive and back to negative indicating presence of secondary vortex on upstream of protrusion. The change in the sign of the skin friction is attributable to fact that this vortex circulates in the opposite sense to that of the primary vortex, causing positive shear. Such phenomenon is not noticed in the $Re_\infty=10^3$ as well as 10^4 . As the Reynolds number increases, the separated region shows a plateau of nearly constant pressure more prominently for $Re_\infty=10^5$.

Figures 15a-b show variation of separation lengths (upstream and downstream of protrusion) and peak pressure at the reattachment (stagnation) point on the protrusion with Reynolds number. The peak pressure on the protrusion increases marginally i.e. 68% with an increase in Re by 100 times. In contrast, the separation lengths upstream, downstream, and their sum increase in larger proportions i.e. by 202%, 45% and 151% respectively. We can thus infer that an increase in Reynolds number significantly shifts the shock location. This is in line with the findings by Lewis et al. [14]. The average tangential and normal forces for all three Reynolds numbers are plotted in Fig.16. We observe that the tangential force increases by a factor of 42.89 to 882.79 and the normal force increases from 5.39% to 16.75% (w.r.t. flat plate values). This indicates that the asymmetric force magnitude increases with Re number which suggests placing such protrusion as far as possible from the leading edge i.e tail control rather than canard control.

Effect of Protrusion Shape

Figures 17a-f show the pressure contours and stream traces at for three different shapes of protrusion with same dimensions in height ($RH=8.66\%$) and base width for free stream mach number $M_\infty=4.5$ and Reynolds number $Re=10000$. The only feature different in all three protrusions is the inclination of side wall w.r.t. plate. The inclination being: (1) 60 deg for triangular, (2) 74 deg for trapezoidal, and (3) 90 deg for rectangular shape.

An increase in inclination of side wall or bluntness of protrusion reduces the inclination of all shocks in the flow fields while moves oblique shock-1 towards leading edge and strengths of both oblique shock-1 and 2 increases. Similarly, flow reattaches further downstream for increased wall angle as expected. This results in increase of

the flow separation regions on both sides of the protrusion. Fig. 18a shows the variation of wall pressure as a function of distance from leading edge. The movement of the oblique shock and the associated separation point, towards the leading edge and away from protrusion can be seen. We observe that as the protrusion wall inclination increases, not only does the wall pressure increase (due to pressure jump across shock wave), but this increase starts further upstream. Fig. 18b shows variation of separation lengths (upstream and downstream of protrusion) with protrusion wall inclination. The separation lengths upstream, downstream and their sum increase nearly in linear fashion with increase in protrusion wall angle. The average tangential and normal forces for all three shapes are plotted in Fig. 19. We observe that the tangential force increases by a factor of 351 to 504 and the normal force increases from 19.27% to 28.23% (w.r.t. flat plate values). This indicates that the asymmetric force magnitude increases with protrusion wall angle.

Conclusion

With the long term perspective of using shockwaves created via micro actuated surface protrusions to assist or replace conventional control surfaces in maneuvering of supersonic vehicles and missiles, a detailed computational study of a two dimensional supersonic flow past a flat plate with protrusions of different shapes and sizes is presented. A range of free stream Mach numbers (2.0 - 4.5), Reynolds numbers (1000 - 100000) and protrusion heights (0.866% to 8.66% of the characteristic length) has been considered for a thorough parametric study. The parametric study indicates that the oblique shock structure and strength are influenced by all the variables to varying extents. However, the shock location is substantially altered by the protrusion height, Reynolds number, and protrusion shape, while the influence of Mach number is only marginal. An increase in the protrusion height results in an increased wall pressure as well as increased separation lengths on both sides of the protrusion. In contrast, an increase in Mach number increases the wall pressure, but moves the separation point marginally towards the protrusion. Increase in Reynolds number and protrusion bluntness (triangular \rightarrow trapezoidal \rightarrow rectangular) increases separation lengths on both sides of the protrusion.

With respect to the overall motivation of using surface protrusion generated shock waves as control mechanisms, the feasibility of the concept arises from the force asymmetry due to the presence of the protrusion on only one

side of the flat plate. If the protrusion is deployed only on a need basis, the total drag force over the complete flight envelope will reduce significantly, resulting in a substantially lower propulsive force requirement. With this basic design paradigm in view, the average horizontal and vertical forces on the plate due to pressure and skin friction were calculated during each simulation. The tangential as well as normal forces are observed to increase with increasing protrusion heights, free stream Mach number and free stream Reynolds number. The increase in asymmetric force magnitude with increasing free stream Reynolds number suggests that placing the protrusion as far as possible from the leading edge such as tail control may be recommended (length scale used in the free stream Reynolds number definition is the distance of the protrusion from the leading edge). The asymmetric force magnitude is also found to increase with increasing protrusion bluntness.

The major contributions of the present paper are: (1) mapping of the overall flow field in terms of the principal features - shock creation, shock intersections, formation of separation bubbles, shock boundary layer interaction, etc., (2) detailed look at the flow physics, particularly in the protrusion vicinity, and (3) consideration of important design parameters such as wall pressure, skin friction and the overall normal and tangential force coefficients. Future work will focus on systematically increasing the level of complexity by including the effects of moving protrusions, turbulence and fully three dimensional simulations.

References

1. Anderson, B.H., Jon Tinapple and Lewis Surber., "Optimal Control of Shock Wave Turbulent Boundary Layer Interactions using Micro Array Actuation", 3rd AIAA Flow Control Conference, 5 - 8 June 2006, San Francisco, California.
2. Adam Huang., James Lew., Yong Xu., Yu- Chong Tai and Chih- Ming Ho., "Micro Sensors and Actuators for Macro Fluidic Control", IEEE Sensors Journal, Vol.4. No.4 August, 2004, pp.494-501.
3. Mehul, P. Patel., Javier Lopera and Terry T. Ng., "Active Boat Tailing and Aerodynamic Control Fins for Maneuvering Weapons", 2nd AIAA Flow Control Conference, 28 June to 01 July, 2004, Portland, OR.

4. Smith, F.T., "Laminar Flow Over a Small Hump on a Flat Plate", Journal of Fluid Mechanics, Vol. 57, No.4, March, 1973, pp.803-824.
5. Dolling D.S. and Murphy M.T., "Unsteadiness of the Separation Shock Wave Structure in a Super Sonic Compression Ramp Flow Field", AIAA Journal, Vol.21. No.12, December, 1983, pp.1628-1634.
6. Chapman, D. R., Kuehn, D. M. and Larson, H. K., "Investigation of Separated Flows in Supersonic and Subsonic Streams with Emphasis on the Effect of Transition", NACA TR 1356, 1957.
7. Efimtsov, B. M., Rizzi, S. A., Andersson, A. O. and Andrianov, E. V., "Influence of Small Steps on Wall Pressure Fluctuation Spectra Measured on TU-144LL Flying Laboratory", AIAA Paper 2002-2605, June, 2002.
8. Carter, J.E., "Numerical Solution of the Navier-Stokes Equation for the Supersonic Laminar Flow over Two Dimensional Compression Corner", NASA TR R-385, 1972.
9. Degani, D. and Stegger, J.L., "Comparison Between Navier-Stokes and Thin Layer Computations for Separated Supersonic Flow", AIAA Journal, Vol.21, No.11, 1983, pp.1604-1606.
10. Hung, C. M. and Mac Cormack, R. W., "Numerical Solutions of Supersonic and Hypersonic Laminar Compression Corner Flows", AIAA Journal, Vol.14, No.4, 1976, pp.475-481.
11. Qamar, A., Hasan, N. and Sanghi, S., "New Scheme for the Computation of Compressible Flows", AIAA Journal, Vol.44, No.5, May, 2006.
12. Qamar, A., "Numerical Investigations of the Flow Past Axisymmetric Surface Protuberances Using a New Computational Scheme", Ph.D Thesis, Indian Institute of Technology Delhi, December, 2007.
13. Hoffman, K. A. and Chiang., "Computational Fluid Dynamics for Engineers, Engineering Education System", McGrawHill, New York, 1995.
14. Lewis, J. E., Kubota, T. and Lees, L., "Experimental Investigation of Supersonic Laminar, Two Dimensional Boundary Layer Separation in a Compression Corner with and without Cooling" AIAA Journal, Vol.6, No.1, January, 1968, pp.7-14.
15. Anderson, J. D., Computational Fluid Dynamics, McGrawHill, New York, 1995.
16. Laney, C. B., Computational Gas Dynamics, Cambridge University Press, Cambridge, England, U.K, 1998.

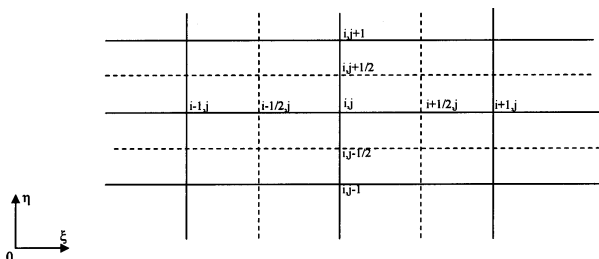


Fig.1 Schematic Diagram Showing Computational Molecule

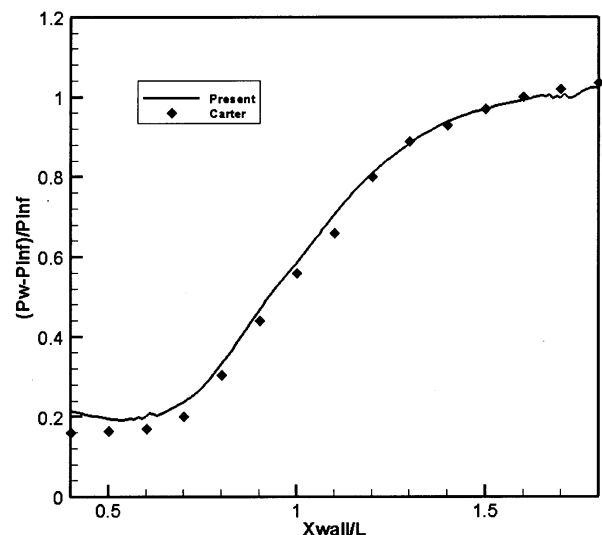


Fig.2 Code and Scheme Validation Study

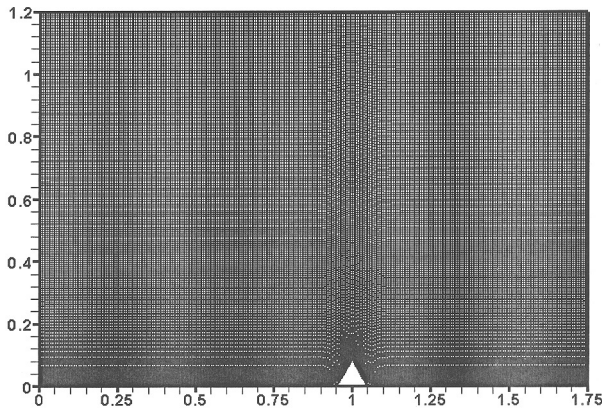


Fig.3 Computational Grid Structure

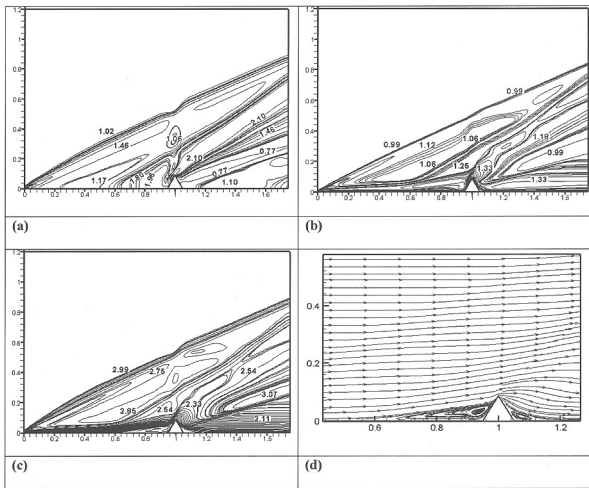


Fig.5 Flow Past the Triangular Protrusion and $M_\infty=3.0$ and $RH=8.66\%$ (a) Pressure Contours, (b) Temperature Contours, (c) Mach Contours, (d) Stream Trace Patterns

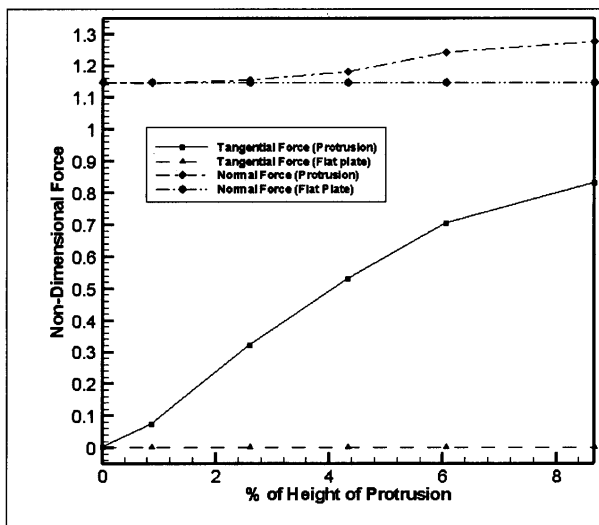


Fig.8 Non-dimensional Normal and Tangential Force Plots for Different Heights of Protrusion

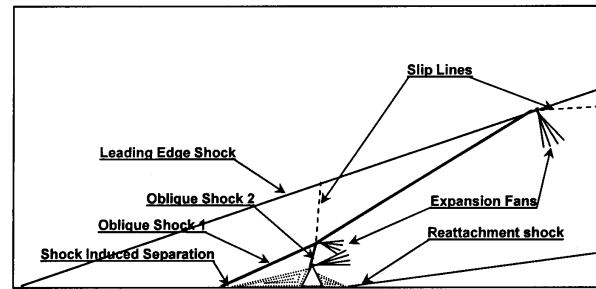


Fig.4 Schematic Diagram of Spatial Flow Features for Supersonic Flow Past Forward-Facing Step

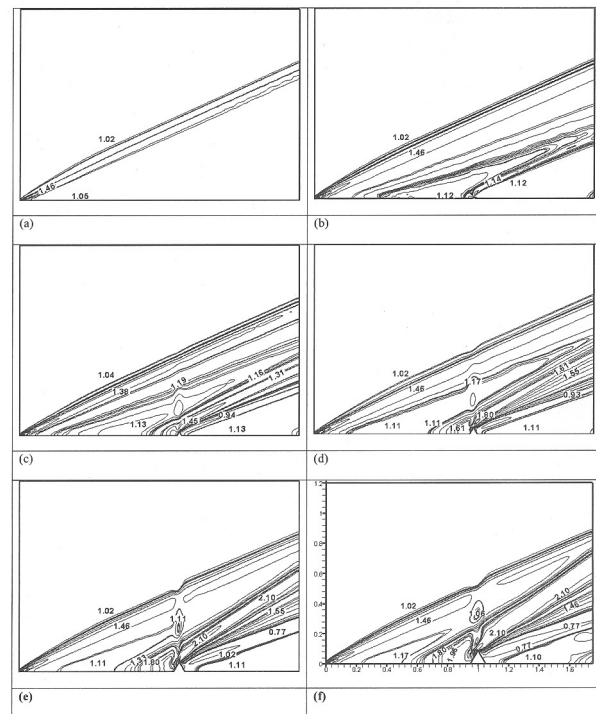


Fig.6 Pressure Contours at $M_\infty=3.0$ for Flow Past the Triangular Protrusion of Heights (a) Flat Plate, (b) $RH=0.866\%$, (c) $RH=2.598\%$, (d) $RH=4.33\%$, (e) $RH=6.06\%$, (f) $RH=8.66\%$

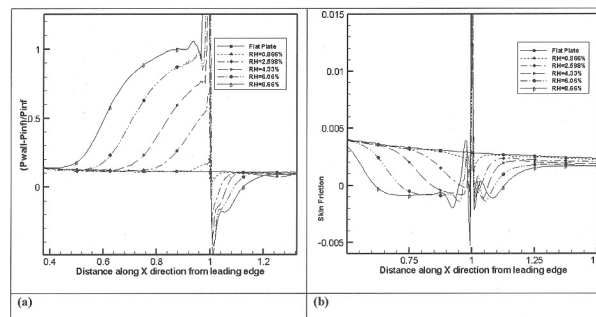


Fig.7 Plots of (a) Pressure, (b) Coefficient of Skin Friction Plots as Compared to Free Stream Pressure for Different Heights of Protrusion

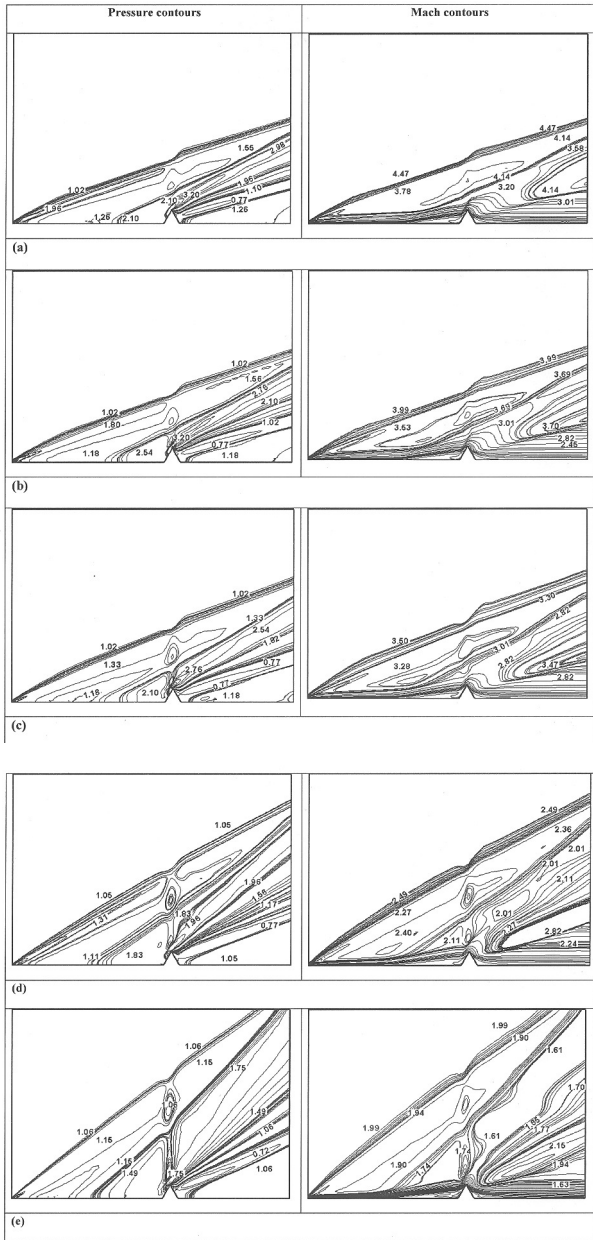


Fig.9 Pressure and Mach Contours Respectively for Flow Past the Triangular Protrusion of Height $RH=8.66\%$ at (a) $Mach=4.5$, (b) $Mach=4.0$, (c) $Mach=3.5$, (d) $Mach=2.5$, (e) $Mach=2.0$

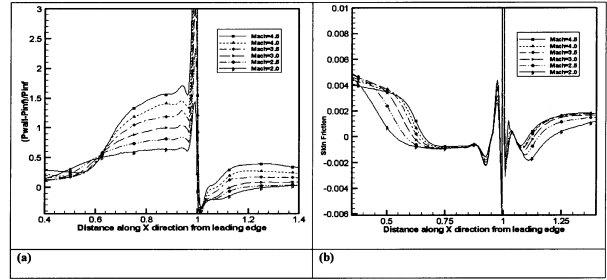


Fig.10 Pressure Plots as Compared to Free Stream Pressure and the Skin Friction Plots for Different Mach No. for $RH=8.66\%$

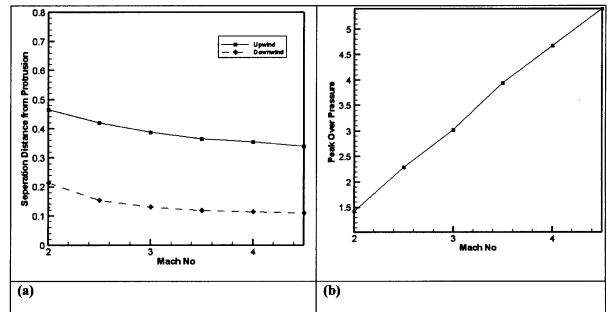


Fig.11 Plots for (a) Separation Distances on Upstream and Downstream Side of the Protrusion, (b) Peak Pressure on the Protrusion for Different Mach No. for $RH=8.66\%$

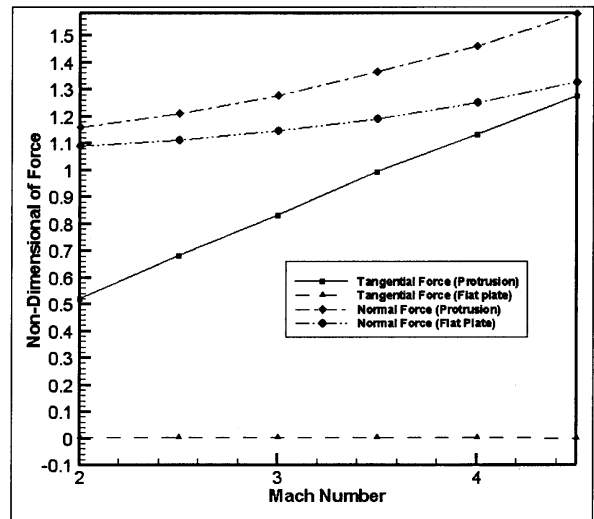


Fig.12 Non-dimensional Normal and Tangential Force for Different Mach No. $RH=8.66\%$ in Comparison with the Flat Plate

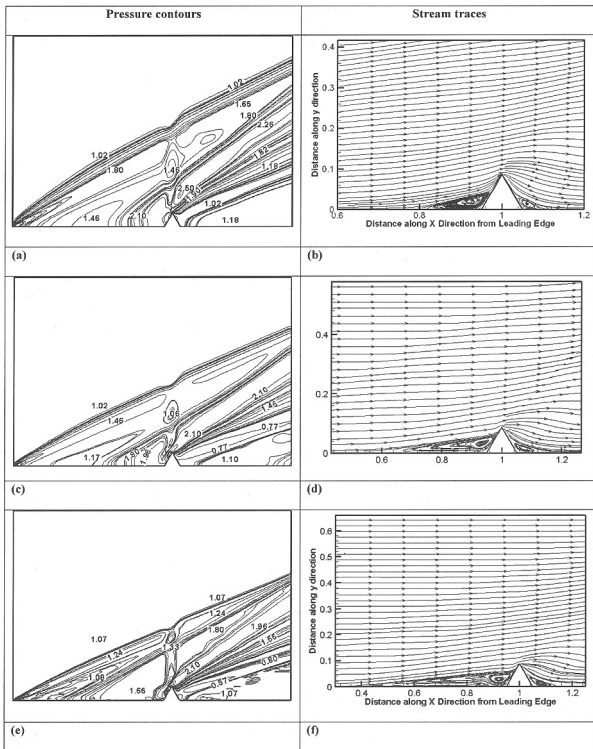


Fig.13 Pressure Contours and Stream Traces for Flow Past the Triangular Protrusion of Height $RH=8.66\%$ for Different Re Numbers

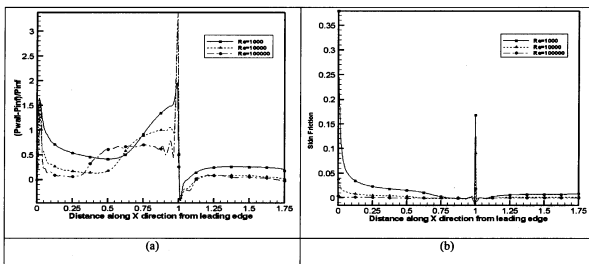


Fig.14 Pressure Plots and the Skin Friction Plots for Different Reynolds No. for $RH=8.66\%$

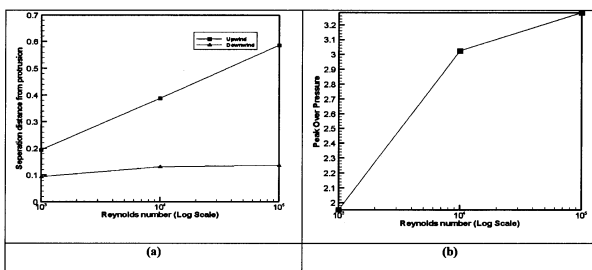


Fig.15 Plots for (a) Separation Distances on Upwind and Downwind Side of the Protrusion, (b) Peak Pressure on the Protrusion for Different Mach No. for $RH=8.66\%$

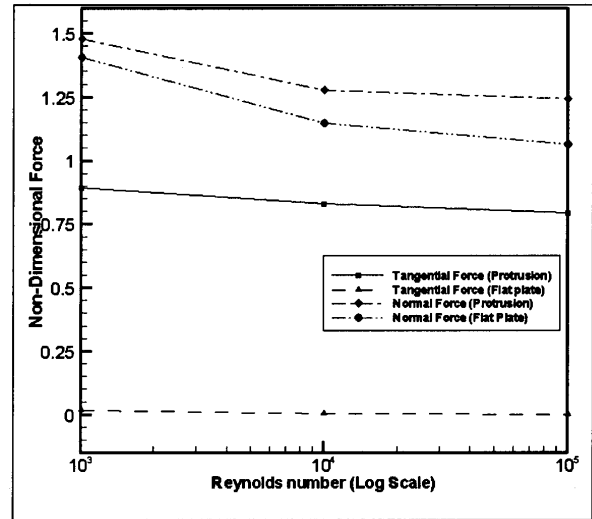


Fig.16 Normal and Tangential Forces for Different Reynolds No. for $RH=8.66\%$ and $Mach=3.0$ in Comparison with the Flat Plate Values

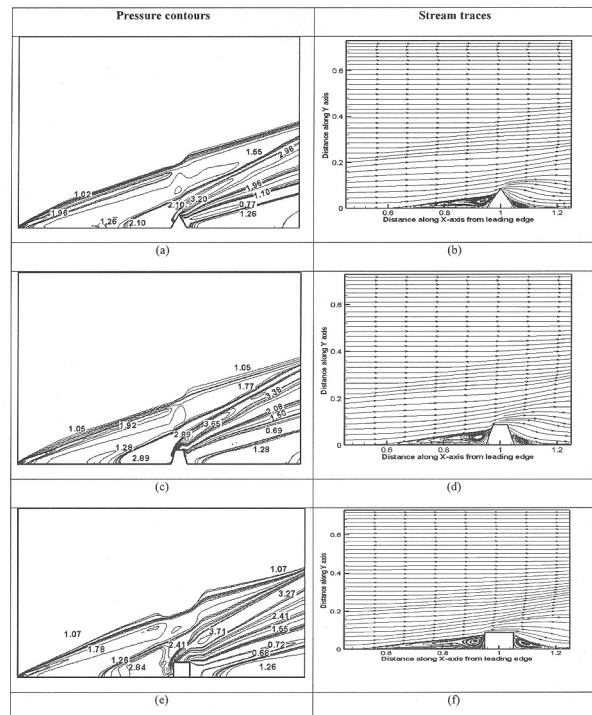


Fig.17 Pressure Contours and Stream Traces for Flow Past the Triangular, Trapezoidal and Rectangular Protrusions of Height $RH=8.66\%$ at $Mach 4.5$ and $Re=10000$ Numbers

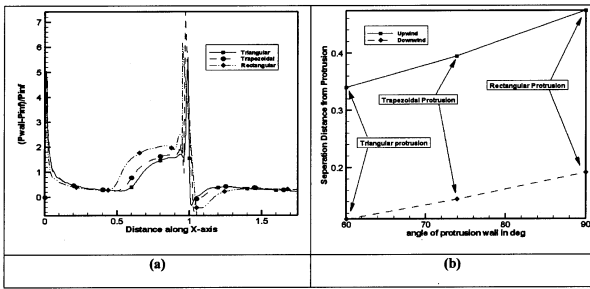


Fig.18 Wall Pressure and Separation Distance Plots for $Re=10000$, $RH=8.66\%$ and $M_\infty=4.5$

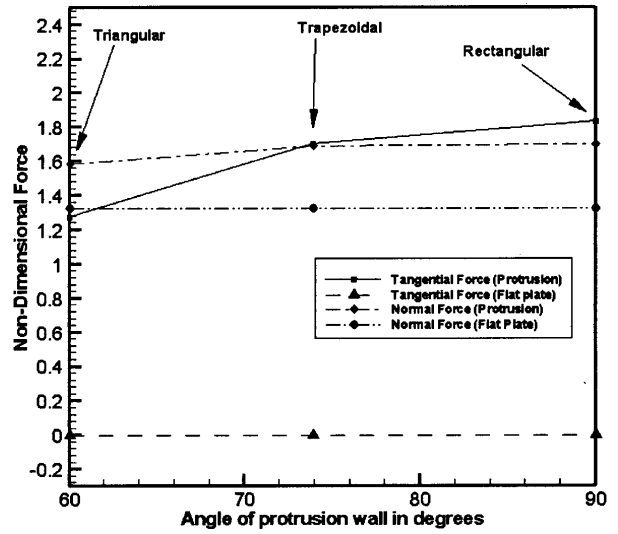


Fig.19 Coefficient Normal and Tangential Force for Different Reynolds No. for $RH=8.66\%$ and $Mach=4.5$ in Comparison with the Flat Plate Values